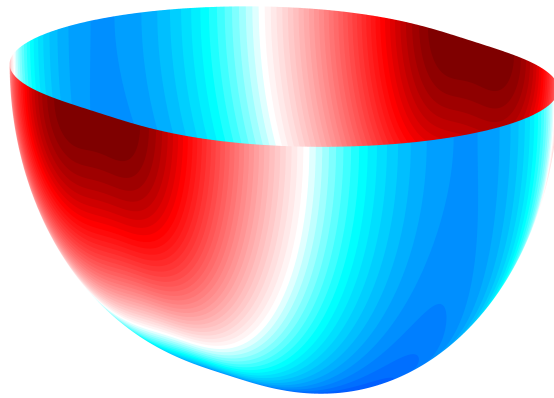




Analysis of Nuclear Magnetic Resonance Force Microscopy



THESIS

submitted in partial fulfillment of the
requirements for the degree of

BACHELOR OF SCIENCE

in

PHYSICS AND MATHEMATICS

Author : Tobias A. de Jong
Student ID : s0881260
Supervisor Physics : M.Sc. Jelmer Wagenaar
Prof. dr. ir. T. H. Oosterkamp
Supervisor Mathematics : Dr. Vivi Rottschäfer

Leiden, The Netherlands, July 15, 2014

Analysis of Nuclear Magnetic Resonance Force Microscopy

Tobias A. de Jong

Huygens-Kamerlingh Onnes Laboratory, Leiden University
P.O. Box 9500, 2300 RA Leiden, The Netherlands

Mathematical Institute Leiden, Leiden University
P.O. Box 9512, 2300 RA Leiden, The Netherlands

July 15, 2014

Abstract

In this thesis an analysis of the resonance slice as found in MRFM experiments is developed and the derived model is used to gain insight in the role of experimental parameters. With this knowledge experiments are proposed to test the model. The influence of the cantilever amplitude and the bandwidth of the RF-pulse according to this analysis are also shown. Lastly a mathematical analysis of partial differential equations arising from spin diffusion in inhomogeneous magnetic fields is performed.

Contents

1	Introduction: Description of the idea MRFM	1
1.1	Motivation	1
1.2	Experimental idea	2
1.2.1	Samples	3
1.3	Theoretical aspects	4
1.3.1	Resonance and slices	4
1.3.2	Signal of a single spin	6
2	Analysis and Simulations	9
2.1	Theoretical work	9
2.1.1	Total signal	9
2.1.2	Slice thickness	10
2.1.3	Requirements for full saturation and adiabatic rapid passage	11
2.1.4	Elaboration and simplification	12
2.1.5	Boundaries of integration	13
2.1.6	Approximations for thickness effects	14
2.2	Numerical results	16
2.2.1	Scaleless results	16
2.2.2	Simulations of experiments	18
2.2.3	Code considerations	24
2.3	Suggested experiments	25
2.4	Discussion	27
3	Spin Diffusion	29
3.1	Motivation for the model	29
3.2	The starting point: the equations of the model	30
3.2.1	Non-dimensionalisation	30

3.3	A Contradiction: amending the equations	32
3.4	Perturbation of the known solution	34
3.5	Solutions in the quasi-static limit	36
3.6	Outlook	39
A	Notation and symbols	41
B	Basic formulae and derivations	43
C	Computer Code	47

Introduction: Description of the idea MRFM

1.1 Motivation

To measure the structure of matter on atomic scale several technologies are nowadays available. Examples include Magnetic Resonance Imaging (MRI), Atomic Force Microscopy variants (STM/AFM) and Nuclear Magnetic Resonance and Electron Spin Resonance (NMR/ESR). However, none of these technologies can give local atomic scale information on the interior of matter: NMR/ESR concern bulk measurements, conventional MRI can not achieve high enough resolution and STM/AFM-like measurements only reach the absolute surface of matter. To achieve this, a cross-over between MRI and AFM was proposed: Magnetic (Resonance) Force Microscopy. Instead of the large scale magnetic field in MRI a single small magnet would be used as both the source of the magnetic field and local probe at the same time. By now, progress has been made as far as the imaging of Tobacco Virus particles [1], the measurement of pure spin transport [2] and spin diffusion [3][4].

Interpretation of the result in MRFM depend on geometrical details of the experiment and thus most publications resort to often quite involved simulations to validate their data, because exact understanding of these geometrical aspects of the measurement methods is far from complete. In this report I will shed light on some facets of the experiments, such as the geometry of the resonance slice, to gain insight into the role of the various aspects. As will be shown in chapter 2 we found some symmetry arguments and relations between parameters which may help to develop

an intuition for the interpretation of simulations and experimental results. We take a slightly different path from that of the group of J. A. Marohn [5], but our results tend to agree and extend upon their earlier results. In chapter 1 we will describe the basics of MRFM and in chapter 3 we attempt an mathematical analysis of spin diffusion.

1.2 Experimental idea

In the Oosterkamp group at Leiden University M(R)FM experiments are done in various experimental setups. Following in the footsteps of Kamerlingh Onnes, we like to think one of our strongest advantages is the fact that we are able to reach temperatures of 10 mK in a cryogenic material free dilution refrigerator with vibrational damping good enough to do atomic scale STM measurements. [6]

Different versions are being developed, but all are based on cantilever oscillation measurements by magnetic flux detection using a SQUID [7]. This as opposed to cantilever oscillation optically detected via interferometry as is done by various other groups. One setup is developed to couple a cantilever with single spins in nitrogen-vacancy complexes in diamond (NV-centres), one to measure on bulk and surface states of for example topological insulators and lanthanum aluminate - strontium titanate interfaces. Also in early development is a setup to measure on biological samples. We will focus on the setup tuned for bulk and surface states, but would like to stress that most of the techniques discussed in this report can be easily adapted to analyse measurements on the other setups.

The general layout of the setup is shown in figure 1.1. A small permanent dipole magnet is attached to the end of an ultrasoft cantilever. The ferromagnet is magnetized in the y -direction, while the primary mode of oscillation of the cantilever is in the x -direction, perpendicular to the magnetic moment. A closed superconducting circuit connects a pick up loop on the sample to a second coil further away. This second coil is coupled to a superconducting quantum interference device (SQUID), which is used as a detection system.

The exact theory of SQUIDs is quite involved, but extensively described in literature. Wijts gives a comprehensive explanation of the relevant pieces in Section 3.3 of his thesis [3], here I will only introduce the vital aspects needed to comprehend the setup. The system detects changes in the local magnetic field, as changes in flux through the pick up loop due to the movement of the magnet induce a small current in the circuit, which in-

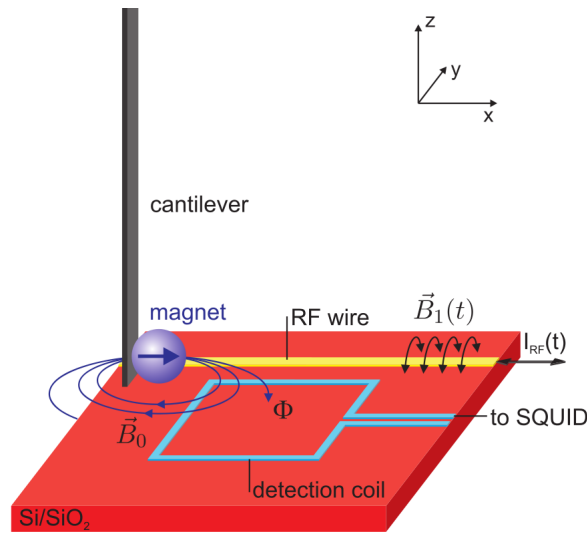


Figure 1.1: Schematic representation of the experimental setup. \vec{B}_0 is the magnetic field of the magnet on the cantilever which gives a flux through the detection coil. An alternating current I_{RF} through the superconducting RF wire induces an electromagnetic field with magnetic component $\vec{B}_1(t)$ to do resonance experiments. Note: The dipole in our setup is actually oriented in the y-direction. This figure is adapted from Wijts' thesis[3].

duces via the second coil a magnetic field through the SQUID. The magnetic flux through the SQUID is quantized in units of $\Phi_0 = \frac{h}{2e}$ due to the two Josephson junctions in the SQUID. This gives a measurable potential variation, as the magnetic flux through the SQUID is countered by a small current. The high sensitivity of the SQUID enables us to measure the resonance frequency of the cantilever with high precision. Thus it is possible to measure the small deviations from this frequency stemming from the interaction between the magnet and the spins in the sample.

It is this interaction we are interested in. Since the magnetic field from the tip is highly spatially variant, very local manipulations of the spins in the sample can be done, as explained in Section 1.3.1. As the measurement system can be sensitive enough to measure these manipulations, this means we can extract information about the local aspects of the spins with a very high resolution.

1.2.1 Samples

The analysis as presented in Part II can be used on various sample types, but we apply it here for a copper sample as made by De Haan and Wa-

genaar, as shown in figure 1.2. This sample will be used as a first test of the setup. The sample is deposited on a silicon substrate through focused ion beam and sputtering techniques. The actual copper sample is $30\mu\text{m}$ by $30\mu\text{m}$ and 300nm thick. The cantilever is an IBM-style cantilever, but without the usual mirror as this is not needed for our measurement method. A spherical NdFeB particle of $3.5\mu\text{m}$ diameter with a magnetisation m_s is attached to the cantilever, in such way that the magnetisation is perpendicular to the primary direction of oscillation and parallel to the sample surface. The sample Wijts used had the same cantilever and magnet, but the sample itself was SrTiO_3 deposited on a silicon substrate.

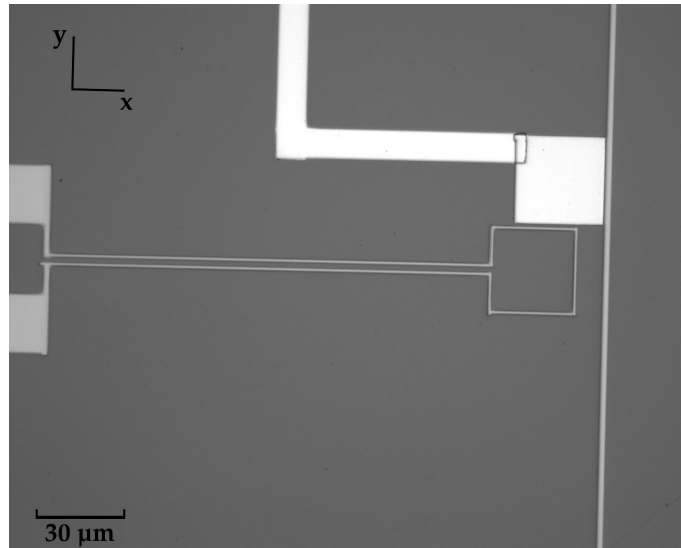


Figure 1.2: An optical microscope image of the sample as Wagenaar and Den Haan use. Visible are the pickup coil (center rectangular grey loop), the copper sample with a grounding wire (white square) and the RF-line (vertical line to the right of the other features).

1.3 Theoretical aspects

1.3.1 Resonance and slices

In a magnetic field the Zeeman-splitting gives rise to an energy difference depending on the orientation of the spin and the magnetic field, proportional to the magnetic field:

$$E - E_0 = -\vec{\mu} \cdot \vec{B} \quad (1.1)$$

Here μ is the magnetic moment of the spin and \vec{B} is the magnetic field. In paramagnetic systems where the spins will align only parallel or anti-parallel (known as 'up' and 'down') to the magnetic field, this reduces to:

$$E - E_0 = -|\vec{\mu}||\vec{B}| \quad (1.2)$$

Or looking at the difference between up and down:

$$\Delta E = E_{\downarrow} - E_{\uparrow} = 2|\vec{\mu}||\vec{B}| \quad (1.3)$$

Photons can interact with this system only if the energy of the photon matches the energy splitting of the Zeeman-system. This is called resonance. Using De Broglie's formula $E_{\text{photon}} = hf$ we have as resonance condition:

$$f_{\text{res}} = \frac{2|\vec{\mu}||B_{\text{res}}|}{h} \quad (1.4)$$

In our case μ is the Bohr magneton or some g -factor (order of magnitude 1) times the nuclear magneton, depending on whether we work with electron spins or nuclear spins. This frequency on which photons and spins can interact is known in NMR as the Larmor frequency. Using the definition of these magnetons ($\mu = \frac{e\hbar}{2m}$) we have:

$$f_{\text{res}} = \frac{ge|B_{\text{res}}|}{\pi m} = \frac{\gamma|B_{\text{res}}|}{2\pi} \quad (1.5)$$

Where e is the elementary charge and m is the mass of the electron or proton and γ is the gyromagnetic ratio. Of course we can only measure on the bulk if the photons can reach the bulk of the material and we are not only interested in the surface properties of our sample. The resulting frequencies are however in the radio regime, for which our sample is transparent, so we do reach the bulk.

Polarization

We define the polarization of an ensemble of spins as the difference between the fraction of spins in the up state and the fraction of spins in the down state. For bulk spins in the described two-level Zeeman system in thermodynamic equilibrium the polarization is given by the Boltzmann polarization:

$$p(T, B) = \frac{\exp\left(\frac{2\mu B}{k_B T}\right) - 1}{\exp\left(\frac{2\mu B}{k_B T}\right) + 1} = \tanh\left(\frac{\mu B}{k_B T}\right) \quad (1.6)$$

In MRFM experiments pulses of RF radiation of a frequency resonant with the local magnetic field B_{res} are used to induce absorption and stimulated emission, resulting in a lowering of the absolute polarization $|p|$. Since the RF radiation is only resonant for one value of B , this only happens in an isomagnetic surface, a surface where the absolute value of the magnetic field is constant, called the resonant slice. If $p = 0$ is reached, we speak of saturation which corresponds to the maximum achievable change and thus maximum signal.

1.3.2 Signal of a single spin

We will now explain the interaction of a single spin and the cantilever. For this system the spin Hamiltonian is given by the Zeeman splitting:

$$H_{spin}(\vec{B}, \vec{\mu}) = -\vec{\mu} \cdot \vec{B}(\vec{r}) \quad (1.7)$$

If we assume that the magnetic moment of the spin is aligned to the local field, this reduces to:

$$H_{spin}(\vec{B}, \vec{\mu}) = \mp \frac{|\vec{\mu}| |\vec{B}(\vec{r})|}{|\vec{B}(\vec{r})|} \cdot \vec{B}(\vec{r}) = \mp |\vec{\mu}| |\vec{B}| \quad (1.8)$$

Where the sign is negative (positive) if the spin and the magnetic field are (anti-)parallel.

We will measure the effects on the cantilever. It can act as a sensitive force sensor, since any external force on the cantilever will influence its potential and thus the oscillation frequency. The force on the spin is given by $\vec{F} = \nabla H_{spin}$. Newton's third law now gives that the force on the cantilever is given by: $\vec{F} = -\nabla H_{spin}$. Since the cantilever primarily moves in the x direction, all relevant forces are those in this direction. Thus we only need to consider the x -component of the force, which equals the x -derivative of $-H$. The effective spring constant is given by (ignoring non-linear effects):

$$F = F_{cantilever} + F_{spin} = (k_{cantilever} + k_{spin})x = kx \quad (1.9)$$

So, taking another derivative in the x -direction we come to a formula for the influence of the spin on the effective spring constant:

$$k_{spin} = \frac{dF_{spin}}{dx} = -\frac{d^2}{dx^2} H_{spin} \quad (1.10)$$

This would lead together with equation (1.8) to $k_{spin} = \frac{d^2}{dx^2} (|\mu|B)$. However since the oscillation of the cantilever, and thus the variation of the

magnetic field direction, takes place on a slower time scale than the precession of the spin, the mean angle between the spin and the magnetic field is a constant of motion and the derivative, which is in the slow time scale, should only work on the second factor in equations (1.7) and (1.8). Thus we find the following equation for the influence of a single spin on the effective spring constant:

$$k_{spinlocal} = \frac{|\mu| \vec{B}(\vec{r})}{|\vec{B}(\vec{r})|} \cdot \frac{d^2 \vec{B}(\vec{r})}{dx^2} \quad (1.11)$$

The shift in effective spring constant is however not what is measured, we measure the effect of this shift on the resonance frequency of the cantilever. From the change in spring constant the shift in the frequency of oscillation can be easily calculated with a first order Taylor perturbation, which is valid for $\frac{k_{spin}}{k_0} \ll 1$. This is equivalent with the statement that the force due to the magnetic interaction with the sample is much smaller than the force due to the stiffness of the cantilever itself, which is certainly the case for us. This gives the following equation:

$$\Delta f = \frac{f_0}{2} \frac{k_{spin}}{k_0} \quad (1.12)$$

Which, combined with equation (1.11), corresponds to the equation derived by Lee for the CERMIT protocol [5].

Typical values for our setup are $f_0 = 3\text{kHz}$ and $k_0 = 10^{-4}\text{Nm}^{-1}$, yielding a conversion factor between k_{spin} and measured frequency shift of $1.5 \cdot 10^7 \text{Hz}/(\text{N/m})$.

Analysis and Simulations

Our goal is to analyse the interaction of the magnetic dipole on the cantilever with the ensemble of spins in the sample. From this we hope to get a more fundamental understanding of the system, and we will devise easily verifiable simulations, calculations and some symmetries. In Section 2.1 the theoretical properties of the measurement system are derived and some further analysis is done to be able to do numerical calculations. In Section 2.2 numerical and qualitative results are presented, experiments to check this analysis and results are proposed in Section 2.3. Finally we discuss advantages and disadvantages of this method.

2.1 Theoretical work

2.1.1 Total signal

In the previous chapter an expression was derived for the influence of a single spin on the cantilever spring constant. However, since we are measuring a sample full of spins, we must sum the signal of a single spin for all spins in resonance in the sample. To do this we make the assumption that the spin density ρ is reasonably high, such that the sample can be considered as a continuum and we can integrate over the entire slice to get the total k_{spin} .

Given the fact that in our setup the magnetic field closely resembles a dipole field which falls off as one gets further away from the dipole, it makes sense to model the slice as a mathematical surface with a certain thickness d_{sl} , which may or may not depend on the location. The signal, as explained in Section 1.3.1, is given by the difference between the equi-

librium polarization and zero. Taking this together we have the following formula for the signal:

$$k_{spin} = p(T, B_{res}) \rho \iint_{resslice} d_{sl} k_{spinlocal} dA \quad (2.1)$$

Where $p(T, B_{res})$ is the spin polarization for the resonant slice, given by equation (1.6). If we now substitute the signal of a single spin from equation (1.11) we have:

$$k_{spin} = p(T, B_{res}) \rho \frac{\mu}{B_{res}} \iint_{resslice} d_{sl} \vec{B} \cdot \frac{d^2 \vec{B}}{dx^2} dA \quad (2.2)$$

The d_{sl} term will be further explored in the following Section. The last aspect missing is the actual shape of the resonance slice, expressed in the actual shape of the integral and integrand. Beforehand it is not clear that the requirement $B = B_{res}$ will lead to a closed form, but in Section 2.1.4 we derive a closed expression.

2.1.2 Slice thickness

Near the slice we can approximate the magnetic field by using a Taylor approximation. Because the resonance slice is an isosurface, the gradient of $|\vec{B}|$ is the normal of the resonance slice. Using again formula (1.4) we can extract the slice widening due to a spread in the frequency of the RF-pulse Δf_{res} . To do this we must however assume that the total width of the slice is small (compared to the magnetic field gradient terms). This is equivalent to the requirement $d_{sl} \ll r_{res}$, since every extra derivative working on $|\vec{B}|$ will give another factor of $1/r_{res}$. This is reasonable, since this condition is nothing more than the requirement that the slice is an actual slice and not a round blob. The Taylor expansion now gives:

$$\Delta f_{res} = \frac{\mu}{h} d_{sl} \left| \nabla |\vec{B}| \right|_{B=B_{res}} + \mathcal{O} \left(d_{sl}^2 \nabla^2 |\vec{B}| \right)$$

Neglecting the higher order terms and rewriting for d_{sl} , we get:

$$d_{sl, \Delta f} = \frac{h \Delta f_{res}}{\mu \left| \nabla |\vec{B}| \right|}$$

Another factor contributing to the slice width is the physical movement of the magnet on the cantilever relative to the sample. This contribution

to the local slice thickness is the inner product between the normal of the surface and the displacement vector. The normal to the surface is given by the direction of the gradient of $|\vec{B}|$. Since the movement of the primary mode of oscillation is in the x -direction, we have:

$$d_{sl, A_{canti}} = \frac{\nabla|\vec{B}|}{|\nabla|\vec{B}||} \cdot \vec{A}_{canti} = \frac{A_{canti}}{|\nabla|\vec{B}||} \left(\nabla|\vec{B}| \cdot \hat{x} \right) = \frac{\frac{\partial|B|}{\partial x}}{|\nabla|\vec{B}||} A_{canti} \quad (2.3)$$

Where A_{canti} is the amplitude of oscillation in the primary direction. Thus we arrive for the contributions of both effects to k_{spin} at the following equations:

$$k_{spin, \Delta f} = p(T, B_{res}) \rho \frac{h\Delta f_{res}}{B_{res}} \iint_{resslice} \frac{1}{|\nabla|B||} \vec{B} \cdot \frac{d^2\vec{B}}{dx^2} dA \quad (2.4)$$

$$k_{spin, A_{canti}} = p(T, B_{res}) \frac{\rho\mu A_{canti}}{B_{res}} \iint_{resslice} \frac{1}{|\nabla|B||} \frac{\partial|B|}{\partial x} \vec{B} \cdot \frac{d^2\vec{B}}{dx^2} dA \quad (2.5)$$

$$k_{spin} = p(T, B_{res}) \frac{\rho\mu}{B_{res}} \iint_{resslice} \left(\frac{h\Delta f_{res}}{\mu} + A_{canti} \frac{\partial|B|}{\partial x} \right) \frac{\vec{B}}{|\nabla|B||} \cdot \frac{d^2\vec{B}}{dx^2} dA \quad (2.6)$$

Where equation (2.4) and (2.5) give the contributions and equation (2.6) gives the combination.

2.1.3 Requirements for full saturation and adiabatic rapid passage

The amplitude of the cantilever oscillation can be tuned, as the cantilever oscillation can be driven by a piezoelectric element. The bandwidth of the RF-radiation can be tuned as well, and as such we can vary the slice width and thus the volume of the resonance slice. This raises the question: what are the constraints to reach full saturation in the slice in a reasonable time? A first idea here is to simply look at the energy constraints: the energy fed to the spin system by the RF radiation must be larger than the energy lost via spin-lattice relaxation.

To be able to do adiabatic rapid passage it is necessary to check whether the adiabatic condition is met. The adiabatic condition is given by Abragam [8] as:

$$\frac{dB_0}{dt} \ll \gamma B_1^2 \quad (2.7)$$

Where B_0 is the (amplitude of the) time dependent magnetic field due to the moving tip, γ is the gyromagnetic ratio of the spins in the sample and B_1 is the amplitude of the magnetic field of the RF-wire. Looking at the resonance slice we have the fastest change of B_0 in the middle of the thickness of the resonance slice as the cantilever passes through its centre position. Using the chain rule to evaluate the time derivative, we have:

$$\frac{dB_0}{dt} = \frac{dB_0}{dx} \frac{dx}{dt} = \frac{dB_0}{dx} \frac{d}{dt} [A_{canti} \sin(2\pi f_0 t)]_{t=0} = \frac{dB_0}{dx} A_{canti} 2\pi f_0$$

Approximating the gradient of $|B|$ with the radial derivative (as explained in Section 2.1.6) and substituting this derivative from Appendix B we get:

$$\frac{dB_0}{dt} \leq 3B_{res}/r_{res} A_{canti} 2\pi f_0 \leq \left(\frac{4\pi B_{res}}{\mu_0 m_s} \right)^{1/3} 3B_{res} A_{canti} 2\pi f_0$$

Substituting this in the adiabatic condition 2.7 we have as requirement:

$$\left(\frac{4\pi B_{res}}{\mu_0 m_s} \right)^{1/3} 3B_{res} A_{canti} 2\pi f_0 \ll \gamma B_1^2$$

If we substitute numerical values for the copper sample we have:

$$B_{res}^{4/3} A_{canti} \ll 1.67 \cdot 10^{-3} \text{T}^{2/3} \text{m} B_1^2$$

To be able to apply the adiabatic theorem it is also required that the modulation frequency of the magnetic field of the dipole is much smaller than the Larmor frequency of the B_1 field, which yields:

$$2\pi f_0 \ll \gamma_{cu} B_1$$

$$\frac{6\pi 10^3}{7.1118 \cdot 10^7} \ll B_1$$

$$B_1 \gg 2.66 \cdot 10^{-4} \text{T}$$

2.1.4 Elaboration and simplification

To come to an actual calculation we introduce a coordinate system as mentioned before, where the magnet at the end of the cantilever is positioned at the origin. The sample is assumed to be positioned under the magnet (in the negative z -direction). We use equation (2.2) given in the previous section. However, before we get to an actual number it has to undergo

somewhat more analysis.

We will exploit the fact that $|B|$ is constant in the resonant slice to gain more insight in the equation to calculate k_{spin} . Elaborating on equation (2.2), using spherical coordinates and the analytic expression for the magnetic dipole field, we have the following (a full derivation, definition of the polar coordinates r, θ, ϕ and the dipole field can be found in appendix B):

$$\begin{aligned}\vec{B} \cdot \frac{d^2 \vec{B}}{dx^2} &= |B|^2 \frac{3}{r^4} \left((5x^2 - 2r^2) + \frac{y^2(10x^2 - r^2)}{3y^2 + r^2} \right) \\ &= |B|^2 \frac{3}{r^2} \left((5 \cos^2 \theta \sin^2 \phi - 2) + \frac{\sin^2 \theta \sin^2 \phi (10 \cos^2 \theta \sin^2 \phi - 1)}{3 \sin^2 \theta \sin^2 \phi + 1} \right) \\ &= |B|^2 \frac{3}{r^2} h(\theta, \phi)\end{aligned}$$

Since switching to polar coordinates introduces a factor $r^2 \sin \phi$ in the surface integral, we find:

$$k_{spin} = 3p(T, B_{res})\rho \mu B_{res} \iint_{resslice} d_{sl} h(\theta, \phi) \sin \phi d\theta d\phi \quad (2.8)$$

All information in the signal about the shape of the resonance slice now lies in the integration boundaries of θ and ϕ ! In the next section we will discuss the implications of this.

2.1.5 Boundaries of integration

For a large enough sample θ will run all the way from 0 to 2π .^{*} Sadly, the limits for ϕ are not so simply determined. Since samples are mostly flat, and because the resonant slices are not spherical, the range of ϕ will depend on θ (Illustrated in figure 2.2). But as soon as we have solved this problem, finite depth samples are no challenge any more, since for a sample of depth D the signal will be the difference between an infinite sample at height d and one at height $d + D$. The equation relating the height above the sample d and the edge of the resonance slice at angles ϕ and θ is the following:

$$d = r_{res}(\phi, \theta) \cos \phi$$

^{*}Note that, due to the symmetry in x and y , if the cantilever is positioned above a side or corner of the sample, the signal will simply be respectively halved or quartered. This is quite easily verifiable in experiment and in combination with the knowledge of what parts of the slice contribute positive or negative to the signal.

Rewriting the equation for the dipole field to express r_{res} as a function of location and B_{res} (Appendix B), we come to the following implicit equation for the boundary of integration for ϕ as function of d and θ :

$$d = \cos \phi \sqrt[3]{\frac{\mu_0 m_s}{4\pi B_{res}}} \sqrt[6]{3 \sin^2 \theta \sin^2 \phi + 1}$$

Taking the sixth power of both sides now gives:

$$\left(\frac{\mu_0 m_s}{4\pi B_{res}}\right)^2 (3 \sin^2 \theta \sin^2 \phi + 1) \cos^6 \phi - d^6 = 0$$

Moving the constants to one term, we find a formula describing the implicit dependence of ϕ on θ for the boundary of the integral:

$$(3 \sin^2 \theta \sin^2 \phi + 1) \cos^6 \phi - \left(\frac{4\pi B_{res} d^3}{\mu_0 m_s}\right)^2 = 0 \quad (2.9)$$

This equation is the last one needed to describe the resonance slice. Since it has no simple analytic solution, we will numerically study what the equations from this section can tell about the resonance slice in the next section.

2.1.6 Approximations for thickness effects

To readily make the simulations of the effects described in Section 2.1.2 some approximations were used. We first (see appendix B) note that the radius of the resonance slice is not wildly varying:

$$\left(\frac{\mu_0 m_s}{4\pi B_{res}}\right)^{1/3} 1 \leq r_{res} \leq \left(\frac{\mu_0 m_s}{4\pi B_{res}}\right)^{1/3} (4)^{1/6}$$

Which is equivalent to:

$$1 \leq r_{res} \left(\frac{\mu_0 m_s}{4\pi B_{res}}\right)^{-1/3} \leq 2^{1/3} \approx 1.26$$

Since the resonant slice resembles a (part of a) spheroid it makes sense to estimate the gradient of $|\vec{B}|$ with the derivative in the r -direction. To do this properly we need an upper bound to the error. To this end we introduce the angle α between the normal of the resonance surface $\hat{n} =$

$\frac{\nabla|B|}{|\nabla|B||}$ and normalized r -vector \hat{r} . Since $|\vec{B}|$ is radial symmetric in the y -axis, we need only look in the xy -plane here. We have:

$$\begin{aligned}\frac{\partial|B|}{\partial r} &= \nabla|B| \cdot \hat{r} = \nabla|B| \cdot (\cos \alpha \hat{n} + \sin \alpha \hat{m}) \\ &= \cos \alpha (\nabla|B| \cdot \hat{n}) + \sin \alpha (\nabla|B| \cdot \hat{m})\end{aligned}$$

Where $\sin \alpha \hat{m}$ is the projection of \hat{r} onto the local in plane coordinate. We use that the normal is parallel to the gradient:

$$= \cos \alpha |\nabla|B|| + \sin \alpha (\nabla|B| \cdot \hat{m})$$

Since this is an isomagnetic surface, we have $\hat{m} \cdot \nabla|B| = 0$, and thus:

$$\frac{\partial|B|}{\partial r} = \cos \alpha |\nabla|B||$$

From the equation for r_{res} in appendix B we define (taking $\phi = \pi$ to again restrict to the xy -plane):

$$f(r, \theta) = r^6 - (\sin^2 \theta + 1)$$

The normal vector can now be expressed as follows:

$$\begin{aligned}\hat{n} &= \frac{1}{|\vec{n}|} \left(\frac{\partial f}{\partial r} dr + \frac{\partial f}{\partial \theta} d\theta \right) \\ &= \frac{6r^5 \hat{r} - \sin(2\theta) \hat{\theta}}{\sqrt{36r^{10} + \sin^2(2\theta)}}\end{aligned}$$

Since $\cos \alpha$ is the projection of \hat{n} on \hat{r} , we have now:

$$\begin{aligned}\cos \alpha &= \frac{6r^5}{\sqrt{36r^{10} + \sin^2(2\theta)}} \\ &= \frac{1}{\sqrt{1 + \frac{\sin^2(2\theta)}{36r^{10}}}} \\ &\geq \frac{1}{\sqrt{1 + \frac{1}{36}}} \approx 0.986\end{aligned}$$

Thus we can reasonably approximate the gradient of B with the r -derivative. (On the symmetry axes this approximation is of course exact.) Again from the appendix we have:

$$\frac{\partial B}{\partial r} = -\frac{3}{r}B$$

$$\left. \frac{\partial B}{\partial r} \right|_{B=B_{res}} \approx -\frac{3B_{res}}{r_{res}}$$

Thus it is reasonable, keeping in mind we introduce an error of at most 1.5% to approximate the gradient term at the isosurface by:

$$\left. \frac{1}{|\nabla|\vec{B}||} \right|_{B=B_{res}} = \frac{r_{res}(\phi, \theta)}{3B_{res}} \quad (2.10)$$

This also justifies the following approximation of equation (2.3):

$$\frac{\nabla|\vec{B}|}{|\nabla|\vec{B}||} \cdot \vec{A}_{canti} = A_{canti} (\hat{n} \cdot \hat{x}) \approx A_{canti} (\hat{x} \cdot \hat{r}) = A_{canti} \cos \theta \sin \phi \quad (2.11)$$

2.2 Numerical results

Since the integrand in equation (2.2) is a purely geometrical function and independent of r_{res} , there are aspects of the resonance slice that do not depend on its size. The next section will explore those aspects before we simulate actual experiments.

2.2.1 Scaleless results

Using equation (2.9), with all constants set equal to 1, as an implicit boundary condition we evaluate the integral for different relative heights using MATLAB (`relativesimulation.m` in appendix C).

It was beyond the scope of this project to do exact calculations/simulations with the extra location dependent terms in the slice thickness as given in paragraph 2.1.2, but from the equations we can derive qualitative statements about their influence. Using the approximations from Section 2.1.6 we can make reasonably accurate simulations to study their influence on the measurements, but as those simulations were done for the applied case of the experiment, they will be given in the next section.

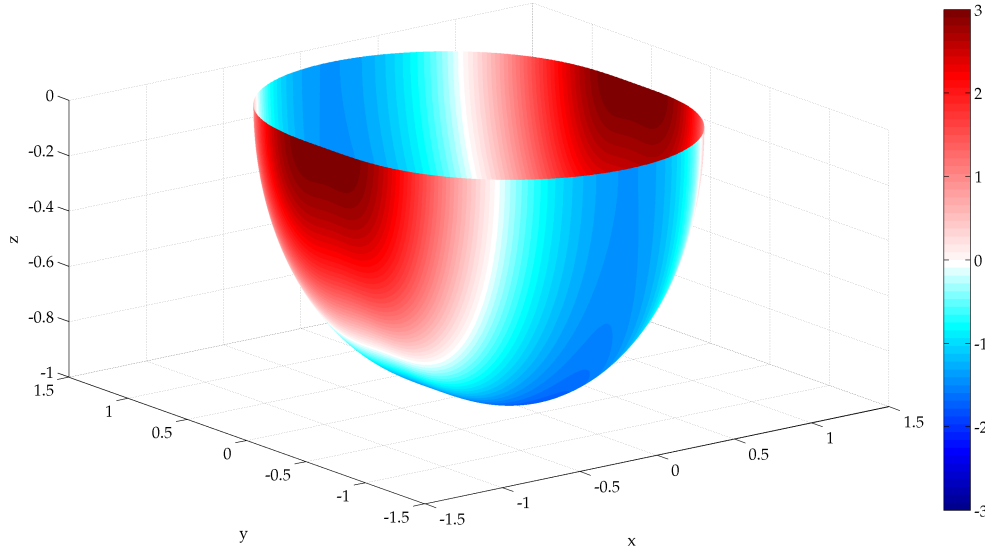


Figure 2.1: The resonant slice as produced by the code in `relativesimulation.m`. Coordinates are as introduced in Section 1.2, so the dipole would be at $(0,0,0)$ oriented in the y -direction. The color corresponds to the local contribution of the slice to the total frequency shift. All scales are relative to the distance between the dipole and the bottom of the resonance slice.

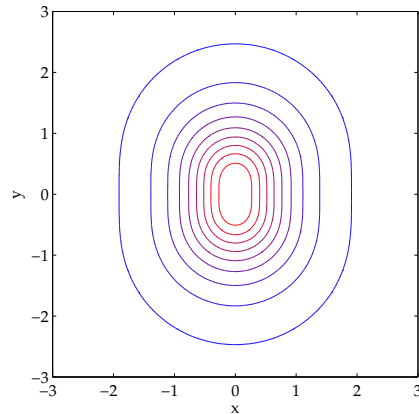


Figure 2.2: Illustration of the shape of the resonant slice at a sample surface for different values of the resonant magnetic field. (Dipole is again oriented in the y -direction, blue is lower B_{res} , red higher, scale is arbitrary)

Since the gradient term can be approximated as given in equation (2.10), it will not vary wildly over a resonance slice and an amplification of the

signal from a larger bandwidth RF-pulse excitation will thus amplify the signal from different parts of the resonance slice quite homogeneously.

The effect of the cantilever movement is however different. Since the cantilever movement is in the x -direction, this will (relatively) amplify the signal from the regions where the resonance slice is perpendicular to x . As one can already see in figure 2.1, this would roughly mean the positive contributing parts of the slice would be amplified relative to the negative contributing parts. As in the next section the overall signal is shown to be negative, the effect of driving the cantilever to larger amplitudes would be at best small or possibly even counter-effective! In figure 2.3 the effect of the pure cantilever movement induced slice thickness is compared to constant slice thickness, the effects of this on the total signal are shown in the next section.

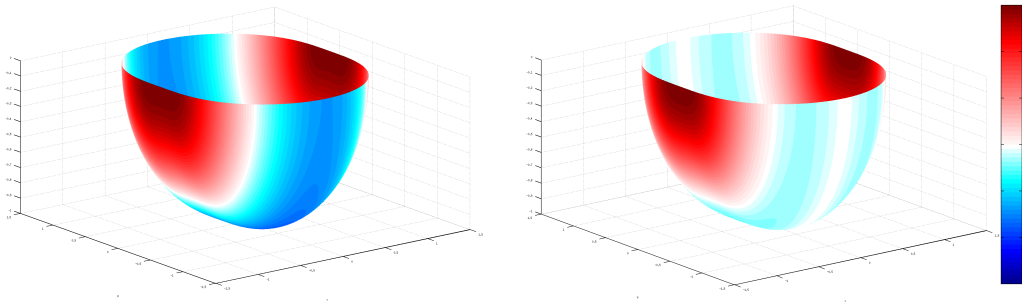


Figure 2.3: Comparison between the local signal contribution with a constant slice thickness (left) and with a slice thickness induced purely by cantilever movement (right, using equation (2.11)). The approximation made for this plot is that the gradient is exactly in the r -direction everywhere on the resonance slice as elaborated in Section 2.1.6.

2.2.2 Simulations of experiments

To get reasonable ranges and some general idea of the values of our variables we substitute numerical values for the constants (as given in appendix A) in the equations for B_{res} and r :

$$B(\phi, \theta, r) = \frac{2.3224 \cdot 10^{-18}}{r^3} \sqrt{3 \sin^2 \theta \sin^2 \phi + 1}$$

$$r_{res}(\pi, \theta) = \sqrt[3]{\frac{\mu_0 m_s}{4\pi B_{res}}} = \frac{1.32 \cdot 10^{-6} \text{T}^{1/3} \text{m}}{\sqrt[3]{B_{res}}}$$

Higher resonance fields yield smaller resonance slices. Taking the distance between the magnet centre and the surface $3.5\mu\text{m}$ we have as maximum value for B_{res} :

$$B_{res}(\pi, \theta, 3.5 \cdot 10^{-6}) = 5.4 \cdot 10^{-2}\text{T}$$

And taking the sample width and length to be $30\mu\text{m}$, using Pythagoras' Theorem and some trigonometry, we have as minimum value for B_{res} to have the slice in our sample for all values of θ :

$$B_{res}\left(\pi + \arctan(3.5/15), 0, \sqrt{3.5^2 + 15^2} \cdot 10^{-6}\right) = 6.4 \cdot 10^{-4}\text{T}$$

As we will see, this means that our sample is effectively infinite in the x - and y -direction if we measure on the middle of the sample. Combining with equation (1.4), we can also get a frequency regime for the RF-field to be resonant with spins in the sample:

$$4.9\text{kHz} \leq f_{res} \leq 4.1 \cdot 10^2\text{kHz}$$

Using again equation (2.9) and combining this with equation (2.8), we can now simulate the signal as function of B_{res} and d as shown in figures 2.4 and 2.5.

All figures of this Section 2.2.2 and Section 2.2.3 use for the non-varying parameters the values as given in Appendix A, unless stated otherwise.

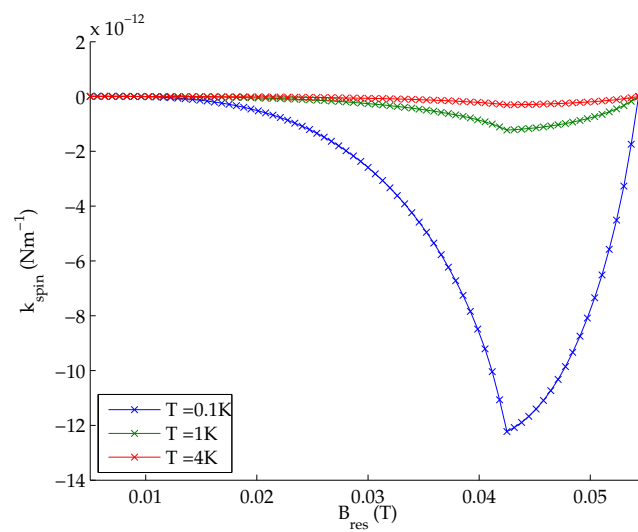


Figure 2.4: The signal as function of the magnetic field corresponding to the resonance frequency as produced by the code in `wrapper.m` (Appendix C). The sharp kink around $B = 0.04T$ is due to the fact that the bottom of the resonance slice moves out of the sample on the underside. Three different temperatures are given, corresponding to different polarizations. Tip height is $3.5 \mu\text{m}$, the simulated sample is 300nm thick.

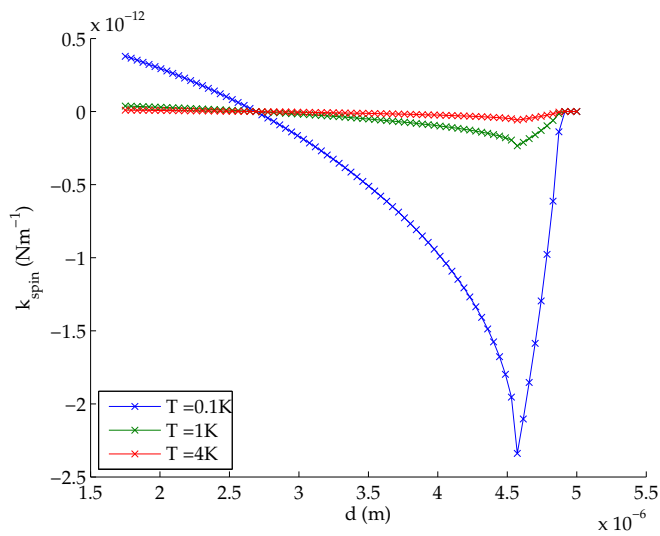


Figure 2.5: The signal as function of height above the sample corresponding to the resonance frequency as produced by the code in `wrapper.m`. Three different temperatures are given, corresponding to different polarizations. Note the similarity with figure 2.4. The difference for low magnetic field/close to the surface, is due to the fact that when varying d , the signal is not quenched by the $p(B_{res}, T)B_{res}$ term. The simulated sample is 300nm thick, RF-field is $B_{res} = 0.02T$. Note that the shape of the curves does not change when B_{res} is altered, only the amplitude and location of the peak will change, as B_{res} is effectively a constant scaling factor in both equation (2.2) and equation (2.9).

Thickness terms

Using the approximations as made in Section 2.1.6 we can alter `mrfmsignal.m` slightly to show the effects of both the cantilever movement and a RF-bandwidth on the signal. In figure 2.6 the results for the influence of the RF-bandwidth on the B -dependency of the signal are shown.

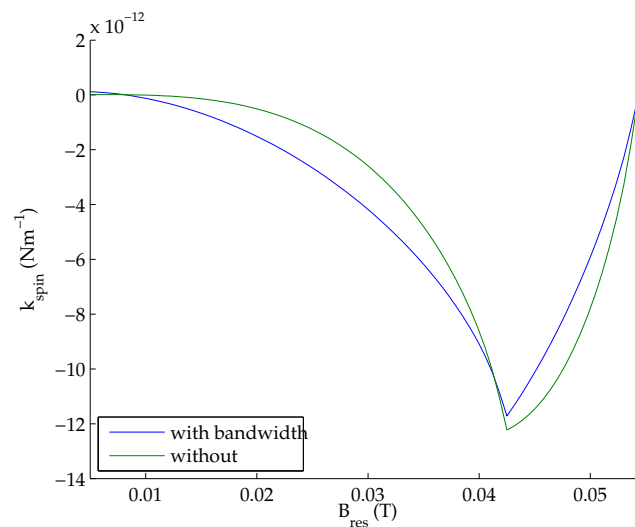


Figure 2.6: The signal as modulated by a finite RF bandwidth as a function of the magnetic field corresponding to the resonance frequency as produced by a slightly modified version of the codes. As one can see there is hardly any difference in the main features of the curve. Tip height is $3.5 \mu\text{m}$, the approximations from Section 2.1.6 were used.

In figures 2.7 and 2.8 the result for the influence of the cantilever movement are shown for different sample thicknesses. As predicted in the previous section the result is more profound, resulting in the shifting of features (in particular the zero crossings) and softening of the peak feature.

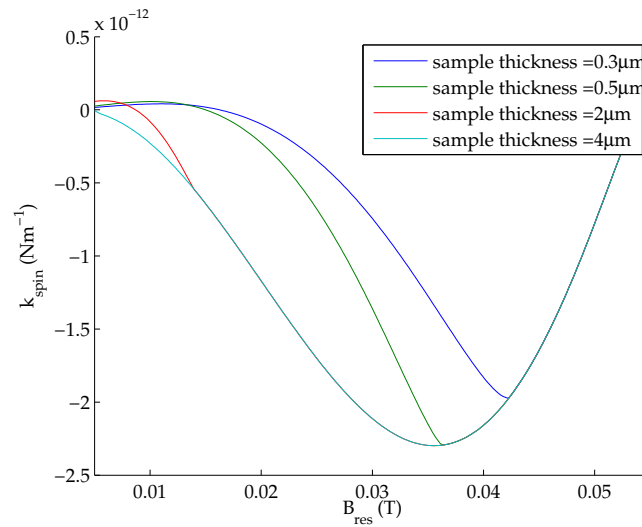


Figure 2.7: The signal as modulated by the movement of the cantilever as a function of the magnetic field corresponding to the resonance frequency as produced by a slightly modified version of the codes. Data for four different sample thicknesses is shown. Tip height is $3.5 \mu\text{m}$, $A_{\text{canti}} = 100\text{nm}$, such that the maximum of d_{sl} is comparable to other figures. The approximations from Section 2.1.6 were used.

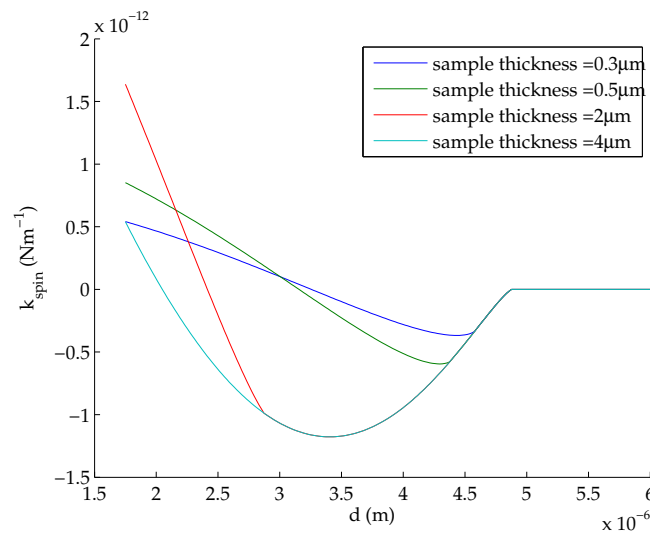


Figure 2.8: The signal as modulated by the movement of the cantilever as a function of height above the sample corresponding to the resonance frequency as produced by a slightly modified version of the codes. Data for four different sample thicknesses is shown. The RF-field is 0.02 T , $A_{\text{canti}} = 100\text{nm}$. The approximations from Section 2.1.6 were used.

2.2.3 Code considerations

Since the code is fully modular, that is, `mrfmsignal.m` (see Appendix C) can be used as a function where all relevant parameters are an input, we can now easily simulate various systems. For example in figure 2.9 we simulate the signal of three stacked layers, each 300 nm thick, giving the signal each of the layers would generate. Or as shown in figure 2.10, even for layers of different thickness. Going even further, one can simulate data for an arbitrary sequence of sets of parameters, making a close comparison to experiments possible.

Since the entire calculation boils down to analytically known factors and one numerical integral, it is easy to verify the numerical error, as MATLAB's built-in routine for integration does adaptive error checking. Default values for absolute tolerance and relative tolerance are respectively 10^{-10} and 10^{-6} , but other values can be set. Also formulae are embedded in the function at one central place, so they can be easily modified or enhanced for future projects.

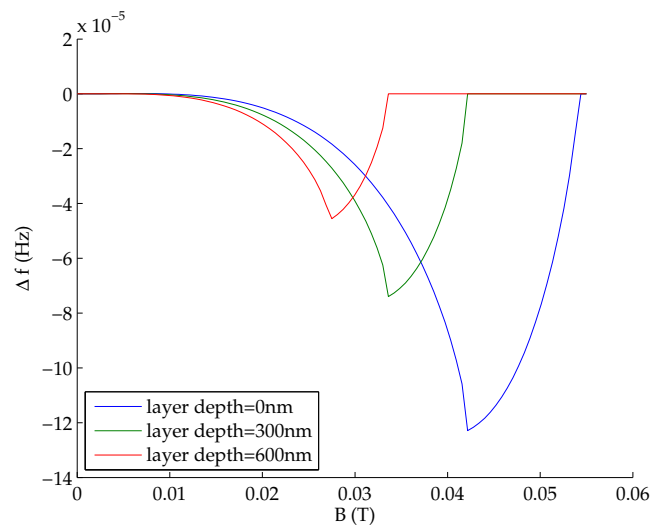


Figure 2.9: The shift in effective spring constant as function of the magnetic field corresponding to the resonance frequency as produced by a slightly altered version of `wrappermultilayer.m`. Each line corresponds to the signal due to one layer of 300nm. Again $d = 3.5\mu\text{m}$. Note that this simulation can be equivalently interpreted as the signal of a 300nm layer at $d = 3.5\mu\text{m}$, $d = 3.8\mu\text{m}$ and $d = 4.1\mu\text{m}$.

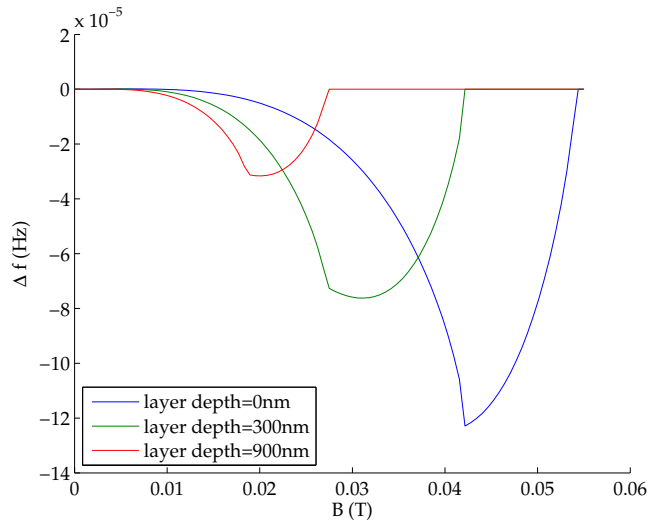


Figure 2.10: The shift in effective spring constant as function of the magnetic field corresponding to the resonance frequency as produced by `wrappermultilayer.m`. Each line corresponds to the signal due to a layer, the deepest two layers 600nm, the top one 300nm. Comparing to figure 2.9, we see that the shape of the curve only depends on the thickness of the layer, the amplitude on the depth. Again $d = 3.5\mu\text{m}$.

2.3 Suggested experiments

Based on the analysis and calculations shown in the preceding sections we propose several experiments below.

Assuming the alignment of the magnet, cantilever and sample is at least reasonable, with the magnetization perpendicular to the primary direction of oscillation and both of these parallel to the sample surface, the sample edges parallel to x and y , our system is symmetrical under reflection in the xz -plane and in the yz -plane. Note that these symmetries also hold if the magnetization is parallel to the oscillation. As mentioned in Section 2.1.5 a good experiment to check these symmetries of the system would be to measure at the middle of the sample, above the edges and above the corners. Leaving all other parameters equal, the signal should be halved on the edges and quartered on the corners.

From the equation for k_{spin} and the equation determining the boundaries of the integral (equations (2.8) and (2.9)), we derive that another worthwhile experiment would be to keep the boundaries of the integral in equation (2.8) constant. From (2.9) we see that the following proportionality

would have to be held:

$$B_{res} \propto d^{-3}$$

Using this the total signal would be:

$$k_{spin} \propto p(T, B_{res}) B_{res} d_{sl}$$

This would give a signal as shown in figure 2.11. As the only term not fully known here is d_{sl} , the deviation from a fit with d_{sl} constant would give an idea of the different effects of slice broadening as discussed in Section 2.1.2, since although the location (in the resonance slice) dependency is scaleless, the magnitudes of the effects scale differently.

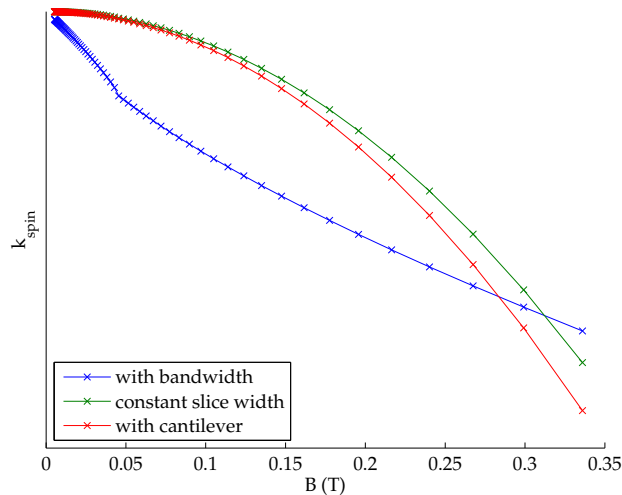


Figure 2.11: The shift in effective spring constant as function of the magnetic field corresponding to the resonance frequency when $B_{res} = 0.042T \cdot (3.5 \cdot 10^{-6} / d)^{-3}$ is fixed. Vertical scale is arbitrary as data has been scaled to comparable magnitude. Data is shown for the RF-bandwidth modulated signal, for the standard signal and for the signal with the effects from cantilever movement shown. (blue, green and red respectively).

The effect of the physical movement of the cantilever on the slice width does not scale with the resonant magnetic field at all, since its magnitude is fully determined by the physical movement of the cantilever. But the effect from the RF bandwidth scales as 1 over the divergence of $|B|$ at B_{res} . Since for the dipole field we have the following:

$$\nabla |\vec{B}| \propto |B|/r \propto |B|^{4/3}$$

We can thus hypothesise that the effects due to RF-bandwidth should scale roughly as $(B_{res})^{-4/3}$ compared to the rest in this experiment, i.e.:

$$k_{spin\Delta f} \propto p(T, B_{res}) B_{res}^{-1/3}$$

This means that by doing this experiment we can experimentally determine the magnitude of the different slice width terms.

2.4 Discussion

The method as discussed has some limitations: it only generally works for systems where the relevant spin Hamiltonian only depends on the magnitude of B , such that we can use this as a constant in the resonant slice. For example the electron resonance experiments on SrTiO_3 as done by Wijts can not be simulated, as the crystal field splitting, which depends on the angle of \vec{B} relative to the crystal of the sample, creates more complex effects such as multiple slices. Another limitation is that the resulting integrals still need to be evaluated numerically, although as mentioned in Section 2.2.3, the error can be adequately controlled.

Spin Diffusion

In this chapter we will do a mathematical analysis of the system of partial differential equations that arises from the problem of spin polarization diffusion in an inhomogeneous magnetic field.

3.1 Motivation for the model

As Vinante et al. concluded in 2011 [4], an important aspect in the understanding of MRFM is how spin polarization diffuses through a sample. The main interaction facilitating this diffusion are flip-flops: in a reasonably homogeneous field two neighbouring opposed spins can interchange their alignment without a large energy mismatch. While this behaviour is well studied both theoretically in the case of a homogeneous magnetic field and using Ising model assumptions and experimentally using MRFM [2], little is known in the continuous limit in an inhomogeneous field. Genack and Redfield [9] derive a set of coupled partial differential equations for the high temperature limit $k_B T \gg \mu B_0$. Both Wijts in his PhD thesis [3] and Vinante et al. in the supplement of their article [10] derive a set of coupled partial differential equations describing the behaviour for the low temperature limit, since for electron spins in applied fields up to a fraction of a Tesla at milliKelvin temperatures this is a valid assumption. Here we will further elaborate on these equations and look at fundamental properties arising from them.

3.2 The starting point: the equations of the model

The system of coupled partial differential equations as derived by Wijts are as follows: *

$$\begin{aligned}\frac{\partial M(x, t)}{\partial t} &= -\frac{\partial}{\partial x} J_m(x, t) - \frac{1}{T_1} (M(x, t) - M_{eq}(x)) \\ \frac{\partial E(x, t)}{\partial t} &= J_m(x, t) \frac{\partial B(x)}{\partial x} + D_d \frac{\partial^2}{\partial x^2} E(x, t) - \frac{1}{T_1} (E(x, t) - E_{eq}(x)) \\ J_m(x, t) &= -D \left(\frac{\partial M(x, t)}{\partial x} + \frac{M^2(x, t)}{\rho \mu B_{loc}} \frac{\partial B(x)}{\partial x} + \frac{E(x, t)}{B_{loc}^2} \frac{\partial B(x)}{\partial x} \right) \\ M_{eq}(x) &= \rho \mu \tanh \left(\frac{\mu B_0(x)}{k_B T_L} \right) \\ E_{eq}(x) &= -\rho \mu B_{loc} \left(1 - \frac{1 - \frac{\mu B_{loc}}{k_B T_L}}{\cosh \left(\frac{\mu B_0(x)}{k_B T_L} \right)} \right)\end{aligned}$$

Where M is the local magnetization, E the local dipole energy, J_m the magnetization flux, ρ the spin density, μ the constant magnetic moment of the spins, B_{loc} the amplitude of the local magnetic field due to the neighbouring spins, B_0 the amplitude of the external magnetic field, B the sum of those two, T_1 the spin-lattice relaxation time, D the diffusion constant related to the diffusion of the magnetization, D_d the diffusion constant related to the dipole energy, k_B Boltzmann's constant and T_L the lattice temperature. x is the (one-dimensional) location variable (not necessarily the x as it is used in part I and II), t the time variable in seconds. Both M_{eq} and E_{eq} are the thermodynamic equilibrium values for respectively M and E based on the energy differences between the up- and down states of the spins due to the (location dependent) magnetic field.

3.2.1 Non-dimensionalisation

Although it can be beneficial in physics to keep all the constants in the equations for the benefit of quick estimation, in this chapter we adapt a dimensionless notation to reduce the number of constants in the equations to simplify the grasp of the mathematical concepts hidden in the equations.

*Some missing dependencies were added for notational completeness

To achieve this we first introduce some constants, allowing us to rewrite the system of equations as: (For the time being we drop the dependencies for legibility reasons)

$$\begin{aligned}\frac{1}{D} \frac{\partial M}{\partial t} &= -\frac{1}{D} \frac{\partial J_m}{\partial x} - \gamma (M - M_{eq}) \\ \frac{1}{D} \frac{\partial E}{\partial t} &= \frac{1}{D} J_m A + \beta \frac{\partial^2 E}{\partial x^2} - \gamma (E - E_{eq}) \\ J_m &= -D \left(\frac{\partial M}{\partial x} + \alpha M^2 A + \delta E A \right)\end{aligned}$$

Where the constants are defined as:

$$\begin{aligned}\alpha &= \frac{1}{B_{loc} \rho \mu}, \quad \beta = \frac{D_d}{D}, \quad \gamma = \frac{1}{T_1 D}, \quad \delta = \frac{1}{B_{loc}^2} \\ A(x) &= \frac{\partial B(x)}{\partial x}\end{aligned}$$

We now introduce a time scaling as $\tau = Dt$, such that $\frac{1}{D} \frac{\partial}{\partial t} = \frac{\partial}{\partial \tau}$, yielding:

$$\begin{aligned}\frac{\partial M}{\partial \tau} &= -\frac{1}{D} \frac{\partial J_m}{\partial x} - \gamma (M - M_{eq}) \\ \frac{\partial E}{\partial \tau} &= \frac{1}{D} J_m A + \beta \frac{\partial^2 E}{\partial x^2} - \gamma (E - E_{eq}) \\ J_m &= -D \left(\frac{\partial M}{\partial x} + \alpha M^2 A + \delta E A \right)\end{aligned}$$

To scale out as many constants as possible, we want to introduce dimensionless equivalents of M , E , J_m and A . To find these we both used the clustering of the constants around certain terms (for example every J -term carries a D) and the physical dimensions of the functions and constants. (For example the dipole energy E in units of Joule is divided by the only constant in the equations associated with Joules, μ in J/T . The units of Tesla resulting from this are compensated by dividing by B_{loc}).

Using these methods, we come to the following dimensionless functions:

$$m(x, \tau) = \frac{1}{\rho \mu} M, \quad e(x, \tau) = \frac{1}{B_{loc} \rho \mu} E, \quad j(x, \tau) = \frac{J_m}{D \rho \mu} \quad \text{and} \quad a(x) = \frac{A(x)}{B_{loc}} =$$

$\frac{1}{B_{loc}} \frac{\partial B(x)}{\partial x}$. Thus we obtain the dimensionless system:

$$\frac{\partial m(x, \tau)}{\partial \tau} = -\frac{\partial j}{\partial x} - \gamma(m - m_{eq}) \quad (3.1)$$

$$\frac{\partial e(x, \tau)}{\partial \tau} = ja + \beta \frac{\partial^2 e}{\partial x^2} - \gamma(e - e_{eq}) \quad (3.2)$$

$$j(x, \tau) = -\frac{\partial m}{\partial x} - a(m^2 + e) \quad (3.3)$$

Where $a(x)$ is a given function corresponding to the derivative of the magnetic field, γ and β are dimensionless constants related to the ratios of the different characteristic times, $e(x, \tau)$, $m(x, \tau)$ and $j(x, \tau)$ are the functions of interest and the x -dependent (thermal) equilibrium terms are given by:

$$m_{eq}(x) = \tanh\left(\frac{\mu B_0(x)}{k_B T_L}\right) = \tanh\left(\frac{\int a(x) dx}{C_L}\right) \quad (3.4)$$

$$e_{eq}(x) = \frac{1 - \frac{\mu B_{loc}}{k_B T_L}}{\cosh^2\left(\frac{\mu B_0(x)}{k_B T_L}\right)} - 1 = (C_L - 1) \frac{1}{a} \frac{\partial}{\partial x} m_{eq} - 1 \quad (3.5)$$

Where we have introduced C_L , a function related to the lattice temperature, which is constant here. (Assuming $B_0(x) = B(x)$)

From the physical meaning of originally E and M we can also derive some information of the codomain of both m and e :

Since the number of spins and their location is fixed in this model and all spins must be either in up or down state, there is both a maximum and a minimum to M . In the dimensionless system this corresponds to:

$$-1 \leq m(x) \leq 1$$

There must be such a limit for e as well, but we can not be more precise, than stating that the energy can either be fully lowered, corresponding to all spins aligning to the field B_{loc} of their neighbours or fully heightened by all being disaligned, corresponding to:

$$-1 \leq e \leq 1$$

3.3 A Contradiction: amending the equations

We now look for stationary solutions. One would assume the statistical equilibrium solutions would be a good guess for this. We will set the

time derivatives to zero and substitute the statistical equilibrium solutions. Rewriting equation (3.5) we have:

$$e_{eq}(x) = (C_L - 1) \frac{1}{a} \frac{\partial}{\partial x} m_{eq} - 1$$

So when we multiply by a we get:

$$ae_{eq} = (C_L - 1) \frac{\partial m_{eq}}{\partial x} - a$$

Setting $e = e_{eq}$ and $m = m_{eq}$ and substituting this in equation (3.1) we find:

$$\begin{aligned} 0 &= \frac{\partial m_{eq}}{\partial \tau} = \frac{\partial}{\partial x} \left(\frac{\partial m_{eq}}{\partial x} + am_{eq}^2 + (C_L - 1) \frac{\partial m_{eq}}{\partial x} - a \right) - 0 \\ &= \frac{\partial}{\partial x} \left(\frac{\partial m_{eq}}{\partial x} C_L + a(m_{eq}^2 - 1) \right) \end{aligned}$$

Integrating with respect to x and setting the integration constant equal to zero (corresponding to zero flux $j = 0$), we obtain a separable ODE:

$$\frac{\partial m_{eq}}{\partial x} C_L = a(1 - m_{eq}^2)$$

So we separate terms to get:

$$\frac{1}{1 - m_{eq}^2} \frac{\partial m_{eq}}{\partial x} = \frac{a}{C_L}$$

And integrate both sides, yielding:

$$\tanh^{-1}(m_{eq}) = \frac{\int a dx}{C_L} = \frac{B}{B_{loc} C_L}$$

Which is consistent with the definition of m_{eq} derived from statistical physics. If we now look at the equation for e_{eq} , we have:

$$\frac{\partial e_{eq}}{\partial \tau} = 0 + \beta \frac{\partial^2 e_{eq}}{\partial x^2} - 0$$

Since the left-hand side equals zero, so does the right-hand side, so we arrive at an inconsistency with equation (3.5):

$$\frac{\partial^2 e_{eq}}{\partial x^2} = 0$$

It seems reasonable that this second derivative of e should be compared to the equilibrium solution, so for now we assume that the correct (amended) equations are:

$$\frac{\partial m(x, \tau)}{\partial \tau} = -\frac{\partial j}{\partial x} - \gamma(m - m_{eq}) \quad (3.6)$$

$$\frac{\partial e(x, \tau)}{\partial \tau} = ja + \beta \frac{\partial^2 (e - e_{eq})}{\partial x^2} - \gamma(e - e_{eq}) \quad (3.7)$$

$$j(x, \tau) = -\frac{\partial m}{\partial x} - a(m^2 + e) \quad (3.8)$$

Where we have added a e_{eq} term in the middle term on the right-hand side of equation (3.7), as this amendment alleviates the inconsistency and gives $m = m_{eq}$, $e = e_{eq}$ and $j = 0$ as a stationary solution.

3.4 Perturbation of the known solution

To obtain the stationary solution in the previous section, we assumed zero flux j . To find solutions with non-zero flux, we assume a small flux $\epsilon j_0(x)$ and a constant (equivalent to B linear in x). We perturb from the known solution. We introduce $\tilde{e} = e - e_{eq}$ and assume the perturbed solutions will be of the following form:

$$\begin{aligned} j &= 0 + \epsilon j_1(x) + h.o.t. \\ \tilde{e} &= 0 + \epsilon^{\zeta} e_1(x) + h.o.t. \\ m &= m_{eq} + \epsilon^{\eta} m_1(x) + h.o.t. \end{aligned}$$

Where ζ and η are strictly positive constants to be determined by the matching conditions, and *h.o.t.* stands for any terms of higher order in ϵ . Substituting this in equations (3.6), (3.7) and (3.8), we have:

$$\begin{aligned}\epsilon \frac{\partial j_1(x)}{\partial x} &= -\gamma \epsilon^\eta m_1(x) + h.o.t. \\ \epsilon^\zeta \frac{\partial^2 e_1(x)}{\partial x^2} &= \epsilon^\zeta \frac{\gamma}{\beta} e_1(x) - \epsilon \frac{\alpha}{\beta} j_1(x) + h.o.t. \\ \frac{\partial m_{eq}}{\partial x} + \epsilon^\eta \frac{\partial m_1}{\partial x} &= -\epsilon j_1(x) - a \left(m_{eq}^2 + 2\epsilon^\eta m_{eq} m_1 + \epsilon^\zeta e_1 + e_{eq} \right) + h.o.t.\end{aligned}$$

We know the first order terms are a solution of the system, so we can eliminate those from the last equation:

$$\epsilon^\eta \frac{\partial m_1}{\partial x} = -\epsilon j_1(x) - a \left(2\epsilon^\eta m_{eq} m_1 + \epsilon^\zeta e_1 \right) + h.o.t.$$

We match $\eta = \zeta = 1$, resulting in the following linear system at order ϵ :

$$\begin{aligned}\frac{\partial j_1(x)}{\partial x} &= -\gamma m_1(x) \\ \frac{\partial^2 e_1(x)}{\partial x^2} &= \frac{\gamma}{\beta} e_1(x) - \frac{\alpha}{\beta} j_1(x) \\ \frac{\partial m_1(x)}{\partial x} &= j_1(x) - a \left(2m_{eq}(x)m_1(x) + e_1(x) \right)\end{aligned}$$

When we define $y_1 = \beta \frac{\partial e_1}{\partial x}$ and $v_1 = (j_1, m_1, e_1, y_1)^\top$ we have:

$$\frac{dv_1}{dx} = \begin{pmatrix} 0 & -\gamma & 0 & 0 \\ -1 & -2am_{eq}(x) & -a & 0 \\ 0 & 0 & 0 & \frac{1}{\beta} \\ -a & 0 & \gamma & 0 \end{pmatrix} v_1$$

To find the solutions of this system we need to find its eigenvalues λ and eigenvectors \vec{v} , as its general solution will be a linear combination of the following form:

$$\sum_i c_i \vec{v}_i e^{\lambda_i x}$$

Where the $c_i \in \mathbb{R}$ are arbitrary constants to be determined by specific boundary conditions. The matrix has the following characteristic polynomial:

$$P(\lambda) = \lambda^4 + 2am\lambda^3 - \gamma \left(1 + \frac{1}{\beta}\right) \lambda^2 - \gamma \frac{2am}{\beta} \lambda + \gamma \frac{a^2}{\beta} + \gamma^2 \frac{1}{\beta}$$

This polynomial has no obvious roots, so there is no easy way to find the eigenvectors and eigenvalues. We will postpone the treatment of this problem to the next section.

3.5 Solutions in the quasi-static limit

There is another simplification of the equations given in (3.6), (3.7) and (3.8) we can study. We will now look at the solutions for large $|x|$, i.e. x such that $m_{eq} \approx \pm 1$. Substituting this and setting the time derivatives to zero we have:

$$0 = -\frac{\partial j}{\partial x} - \gamma(m \mp 1) \quad (3.9)$$

$$0 = ja + \beta \frac{\partial^2 e - e_{eq}}{\partial x^2} - \gamma(e - e_{eq}) \quad (3.10)$$

$$j(x, \tau) = -\frac{\partial m}{\partial x} - a(m^2 + e) \quad (3.11)$$

We now reintroduce $\tilde{e} = e - e_{eq}$ and $y = \beta \frac{\partial \tilde{e}}{\partial x}$. This gives:

$$\frac{dj}{dx} = -\gamma(m \mp 1) \quad (3.12)$$

$$\frac{dm}{dx} = -j - a(m^2 + \tilde{e} + e_{eq}) \quad (3.13)$$

$$\frac{d\tilde{e}}{dx} = \frac{y}{\beta} \quad (3.14)$$

$$\frac{dy}{dx} = -ja + \gamma\tilde{e} \quad (3.15)$$

For which we write:

$$\frac{dv}{dx} = F(v) \quad \text{with: } v = \begin{pmatrix} j \\ m \\ \tilde{e} \\ y \end{pmatrix} \quad (3.16)$$

Solving now $F(v) = 0$ gives:

$$\begin{aligned} m &= \pm 1 && \text{from (3.12)} \\ y &= 0 && \text{from (3.14)} \\ ja &= \gamma \tilde{e} && \text{from (3.15)} \\ j &= -a(1 + \tilde{e} + e_{eq}) && \text{from (3.13)} \end{aligned}$$

Or, substituting the last equation in the one above it:

$$\begin{aligned} \tilde{e} &= -\frac{1 + e_{eq}}{\frac{\gamma}{a^2} + 1} \\ j &= -a \frac{1 + e_{eq}}{1 + \frac{a^2}{\gamma}} && \text{from (3.15)} \end{aligned}$$

Linearising around this fixed point, we have the following system:

$$\frac{dv}{dx} = \begin{pmatrix} 0 & -\gamma & 0 & 0 \\ -1 & -2am & -a & 0 \\ 0 & 0 & 0 & \frac{1}{\beta} \\ -a & 0 & \gamma & 0 \end{pmatrix} v$$

This matrix we recognise from the previous chapter as equivalent to the system as arising from the approach there. It (still) has the following characteristic polynomial:

$$P(\lambda) = \lambda^4 + 2am\lambda^3 - \gamma \left(1 + \frac{1}{\beta}\right) \lambda^2 - \gamma \frac{2am}{\beta} \lambda + \gamma \frac{a^2}{\beta} + \gamma^2 \frac{1}{\beta}$$

This polynomial has no easy roots, so although a very involved closed form solution exists, we will now use perturbation methods to find approximations of these roots, corresponding to the eigenvalues of the matrix. To do this we make the reasonable assumption that $\gamma \ll 1$, which corresponds to the physical property of a long T_1 time compared to the time scale of the diffusion. We introduce $\lambda = \lambda_0 + \gamma^\alpha \lambda_1 + \mathcal{O}(\gamma^{2\alpha})$, where α is a strictly positive constant to be determined by the matching condition. Looking at the leading order terms, we have:

$$\begin{aligned} \mathcal{O}(1) : \lambda_0^4 + 2am\lambda_0^3 &= 0 \\ \lambda_0 &= 0, \vee \lambda_0 = -2am \end{aligned}$$

We now want to know the first order correction terms to the zero solutions: (Note that all cross terms of the form $\lambda_0^j \lambda_1^k$ drop out as we substitute $\lambda_0 = 0$)

$$\mathcal{O}(\gamma) : \gamma^{4\alpha} \lambda_1^4 + \gamma^{3\alpha} 2am \lambda_1^3 - \gamma^{1+2\alpha} \left(1 + \frac{1}{\beta}\right) \lambda_1^2 - \gamma^{1+\alpha} \frac{2am}{\beta} \lambda_1 + \gamma \frac{a^2}{\beta} + \mathcal{O}(\gamma^2) = 0$$

Since $\alpha > 0$ the following hold: $1 + 2\alpha > 1 + \alpha > 1$ and $4\alpha > 3\alpha$. These terms thus can't be matched, but we match the lowest two: $1 = 3\alpha$. Thus we have:

$$2am \lambda_1^3 + \frac{a^2}{\beta} + \mathcal{O}(\gamma^{4/3}) = 0$$

$$\lambda_1 = - \left(\frac{a}{2m\beta}\right)^{1/3} \vee \lambda_1 = e^{\frac{\pi}{3}i} \left(\frac{a}{2m\beta}\right)^{1/3} \vee \lambda_1 = e^{\frac{5\pi}{3}i} \left(\frac{a}{2m\beta}\right)^{1/3}$$

So for $m = 1$ we have:

$$\lambda_1 = - \left(\frac{a}{2\beta}\right)^{1/3} \vee \lambda_1 = e^{\frac{\pi}{3}i} \left(\frac{a}{2\beta}\right)^{1/3} \vee \lambda_1 = e^{\frac{5\pi}{3}i} \left(\frac{a}{2\beta}\right)^{1/3}$$

And for $m = -1$ we have a phase shift in the complex plane of $+\pi/3$:

$$\lambda_1 = \left(\frac{a}{2\beta}\right)^{1/3} \vee \lambda_1 = e^{\frac{2\pi}{3}i} \left(\frac{a}{2\beta}\right)^{1/3} \vee \lambda_1 = e^{\frac{4\pi}{3}i} \left(\frac{a}{2\beta}\right)^{1/3}$$

So in each case we have two (in leading order) strictly real eigenvalues and two complex eigenvalues, where the real eigenvalues have the opposite sign of m , and the real part of the complex eigenvalues has the same sign as m .

To find approximate eigenvectors we write the following:

$$A = A_0 + \gamma A_1$$

$$\lambda = \lambda_0 + \gamma^{1/3} \lambda_1 + \gamma^{2/3} \lambda_2 + \mathcal{O}(\gamma)$$

$$v = v_0 + \gamma^{1/3} v_1 + \gamma^{2/3} v_2 + \mathcal{O}(\gamma)$$

Yielding the following equations for the first orders:

$$\mathcal{O}(1) : 0 = (A_0 - \lambda_0 I) v_0$$

$$\mathcal{O}(\gamma^{1/3}) : 0 = (A_0 - \lambda_0 I) v_1 + (O - \lambda_1 I) v_0$$

$$\mathcal{O}(\gamma^{2/3}) : 0 = (A_0 - \lambda_0 I) v_2 + (O - \lambda_2 I) v_0 + -\lambda_1 v_1$$

Solving the first order system gives the eigenvectors of A_0 :

$$v_0(-2am) = (0, 1, 0, 0)^\top, \quad v_0(0) = (0, 1, -2m, 0)^\top$$

To use this method to find the first correction terms for the eigenvectors one would need to calculate the eigenvalues upto third order (that is: $\mathcal{O}(\gamma)$) to be able to match with the first correction on A , which is of that same order. This seems to be a quite fruitless exercise, keeping in mind the large number of assumptions we have already made.

3.6 Outlook

After non-dimensionalising and amending the equations, finding solutions by analytical means proved difficult. Beside the trivial equilibrium solution with the assumption of zero flux, no solutions were found. Perturbing this solution with a small flux yielded a four dimensional linear system with non-constant coefficients which proved not particularly easy to solve. However, we trust that although it fell beyond the scope of this project, this analysis can serve as a proper basis to do numerical simulations of this model of spin diffusion.

Appendix A

Notation and symbols

Below are the used symbols and where applicable their numerical values as used in Chapters 1 and 2. Values in brackets give values used in simulations for non-varying parameters.

$m_s = 2.3224 \cdot 10^{-11} \text{Am}^2$	The magnetic moment of the dipole magnet
$\mu_0 = 4\pi \cdot 10^{-7} \text{Tm/A}$	Vacuum permeability
$\mu_N = 5.05078324 \cdot 10^{-27} \text{J/T}$	Nuclear magneton
$\mu_B = 9.27400968 \cdot 10^{-24} \text{J/T}$	Bohr magneton
$\mu = \mu_B \vee \mu = g\mu_N$	Magnetic moment of a spin in the sample
$g_{Cu} = 1.4849$ (1)	g-factor (value used in simulations)
$\rho = 8,8 \cdot 10^{29} \text{m}^{-3}$	Density of spins in copper
$h = 6.62606957 \cdot 10^{-34} \text{Js}$	Planck's constant
$A_{canti} = (100\text{nm})$	Amplitude of the cantilever oscillation
$d = 1.75 - \dots \mu\text{m}$ (3.5 μm)	Distance centre of the dipole - sample surface
$r_{res}(\phi, \theta)$	Distance from O to the resonance slice
$B_{res} = 0.02\text{T}$	Magnetic field corresponding to the RF-frequency

f_{res}	Larmor frequency applied to induce resonance
Δf_{res}	Bandwidth of the RF-frequency
$d_{sl} = (100\text{nm})$	The (local) thickness of the resonance slice
$f_0 = 3\text{kHz}$	Eigenfrequency of oscillation of the cantilever
$k_0 = 10^{-4}\text{Nm}^{-1}$	Spring constant of the cantilever
$T = (0.1\text{K})$	Temperature of sample
$D = (300\text{nm})$	Sample thickness
$\gamma_{Cu} = 71.118 \cdot 10^6\text{rad}(\text{sT})^{-1}$	Gyromagnetic ratio of the copper nucleus

Below are the extra symbols used in Chapter 3.

$m(x, \tau)$	Normalised magnetisation, equivalent to polarization
$e(x, \tau)$	Normalised dipole energy
D	Diffusion constant for magnetization
D_d	Diffusion constant for dipole energy
$\tau = Dt$	Normalised time
T_1	Mean spin-lattice relaxation time
$a = \frac{1}{B_{loc}} \frac{\partial B(x)}{\partial x}$	x -derivative of the normalized magnetic field
$\gamma = \frac{1}{T_1 D}$	Dimensionless ratio between spin-lattice relaxation and diffusion speed
$\beta = \frac{D_d}{D}$	Dimensionless ratio between magnetization and dipole energy diffusion time
$v_1 = (j_1, m_1, e_1, y_1)^\top$	Vector of quantities

Appendix **B**

Basic formulae and derivations

In this appendix the basic formulae and some derivations of mathematical results from the report will be given. The polar coordinates, where θ is defined, as is customary in mathematics, as the angle in the xy -plane and ϕ is the angle with the z -axis:

$$\begin{aligned}r^2 &= x^2 + y^2 + z^2 \\x &= r \cos \theta \sin \phi \\y &= r \sin \theta \sin \phi \\z &= r \cos \phi\end{aligned}$$

The components of the magnetic dipole field \vec{B} are:

$$\begin{aligned}B_x &= \frac{\mu_0 m_s}{4\pi} \frac{3xy}{r^5} \\B_y &= \frac{\mu_0 m_s}{4\pi} \frac{3y^2 - r^2}{r^5} \\B_z &= \frac{\mu_0 m_s}{4\pi} \frac{3zy}{r^5}\end{aligned}$$

The magnitude of the dipole field:

$$\begin{aligned}|\vec{B}|(y, r) &= \frac{\mu_0 m_s}{4\pi r^4} \sqrt{3y^2 + r^2} \\|\vec{B}|(\phi, \theta, r) &= \frac{\mu_0 m_s}{4\pi r^4} \sqrt{3r^2 \sin^2 \theta \sin^2 \phi + r^2} \\&= \frac{\mu_0 m_s}{4\pi r^3} \sqrt{3 \sin^2 \theta \sin^2 \phi + 1}\end{aligned}$$

Some first derivatives:

$$\begin{aligned}\frac{\partial |\vec{B}|}{\partial r} &= -\frac{3\mu_0 m_s}{4\pi r^4} \sqrt{3 \sin^2 \theta \sin^2 \phi + 1} \\ &= -\frac{3}{r} B \\ \frac{\partial |\vec{B}|}{\partial \theta} &= -\frac{3\mu_0 m_s}{4\pi r^4} \frac{3 \sin^2 \phi \sin \theta \cos \theta}{\sqrt{3 \sin^2 \theta \sin^2 \phi + 1}} \\ \frac{\partial |\vec{B}|}{\partial \phi} &= -\frac{3\mu_0 m_s}{4\pi r^4} \frac{3 \sin^2 \theta \sin \phi \cos \phi}{\sqrt{3 \sin^2 \theta \sin^2 \phi + 1}}\end{aligned}$$

And some second derivatives:

$$\begin{aligned}\frac{d^2 B_x}{dx^2} &= \frac{\mu_0 m_s}{4\pi} \frac{15xy(7x^2 - 3r^2)}{r^9} \\ \frac{d^2 B_y}{dx^2} &= \frac{\mu_0 m_s}{4\pi} \frac{3(35x^2 y^2 + 5z^2 r^2 - 4r^4)}{r^9} \\ &= \frac{\mu_0 m_s}{4\pi} \left(\frac{15y^2(7x^2 - r^2)}{r^9} + \frac{3(r^2 - 5x^2)}{r^7} \right) \\ \frac{d^2 B_z}{dx^2} &= \frac{\mu_0 m_s}{4\pi} \frac{15zy(7x^2 - r^2)}{r^9}\end{aligned}$$

Taking $B = B_{res}$ constant we can express the radius as a function of ϕ and θ :

$$r_{res}(\phi, \theta) = \left(\frac{\mu_0 m_s}{4\pi B_{res}} \right)^{1/3} \left(3 \sin^2 \theta \sin^2 \phi + 1 \right)^{1/6}$$

In Section 2.1.4 we use a result of the following derivation:

We start with filling in the components and second derivatives in Cartesian coordinates:

$$\begin{aligned}\vec{B} \cdot \frac{d^2 \vec{B}}{dx^2} &= \left(\frac{\mu_0 m_s}{4\pi} \right)^2 \frac{1}{r^{14}} \left(3xy \cdot 15xy(7x^2 - 3r^2) + \right. \\ &\quad \left. + (3y^2 - r^2) \cdot 3(35x^2 y^2 + 5z^2 r^2 - 4r^4) + 3zy(15zy(7x^2 - r^2)) \right)\end{aligned}$$

A lot of reordering of terms:

$$\begin{aligned}
&= \left(\frac{\mu_0 m_s}{4\pi}\right)^2 \frac{3}{r^{14}} \left(15x^2 y^2 (7x^2 - 3r^2) + \right. \\
&\quad \left. + (3y^2 - r^2) \cdot (5(7x^2 y^2 + z^2 r^2) - 4r^4) + 15z^2 y^2 (7x^2 - r^2)\right) \\
&= \left(\frac{\mu_0 m_s}{4\pi}\right)^2 \frac{1}{r^{14}} \left(45y^2 r^2 (5x^2 - r^2) - 15y^2 r^2 (7x^2 - r^2) \right. \\
&\quad \left. - 9y^2 r^2 (5x^2 - r^2) + 3r^4 (5x^2 - r^2)\right) \\
&= \left(\frac{\mu_0 m_s}{4\pi}\right)^2 \frac{3}{r^{12}} \left(12y^2 (5x^2 - r^2) - 5y^2 (7x^2 - r^2) + r^2 (5x^2 - r^2)\right) \\
&= \left(\frac{\mu_0 m_s}{4\pi}\right)^2 \frac{3}{r^{12}} \left((7y^2 + r^2)(5x^2 - r^2) - 10y^2 x^2\right)
\end{aligned}$$

We reintroduce a term $|B|^2$, which gives a denominator:

$$= |B|^2 \frac{3}{r^4} \frac{(7y^2 + r^2)(5x^2 - r^2) - 10y^2 x^2}{3y^2 + r^2}$$

Which we try to compensate as much as possible:

$$\begin{aligned}
&= |B|^2 \frac{3}{r^4} \frac{(5x^2 - 2r^2)(3y^2 + r^2) + y^2(10x^2 - r^2)}{3y^2 + r^2} \\
&= |B|^2 \frac{3}{r^4} \left((5x^2 - 2r^2) + \frac{y^2(10x^2 - r^2)}{3y^2 + r^2} \right)
\end{aligned}$$

We reintroduce spherical coordinates and gather all r terms:

$$= |B|^2 \frac{3}{r^2} \left((5 \cos^2 \theta \sin^2 \phi - 2) + \frac{\sin^2 \theta \sin^2 \phi (10 \cos^2 \theta \sin^2 \phi - 1)}{3 \sin^2 \theta \sin^2 \phi + 1} \right)$$

Since all terms share the same power of r , we can introduce a function $h(\theta, \phi)$:

$$= |B|^2 \frac{3}{r^2} h(\theta, \phi)$$

So by introducing the term $|B|^2$ we achieved that only a $1/r^2$ factor is left as r -dependency. This means that in an integral in spherical coordinates as in equation (2.8) all r -dependencies cancel.

Appendix C

Computer Code

relativesimulation.m

This code is used to generate (visualisations of) scaleless results as in Section 2.2.1. It forms the basis of `mrfmsignal.m`, but uses no numerical values and has added code to generate the actual plots of the resonance slice and do some sanity checks.

```
1 function [fighandles] = relativesimulation(symmap)
2 %Calculates the expected Kspin signal assuming full saturation using a
3 %dimensionless integral over the analytic expression g(t,p). The analytic
4 %formula for kspin is also used to generate visualizations of the local
5 %signal in the slice.
6 %Code is written by Tobias de Jong. Last edited: 12 June 2014
7 r = @(t,p) (3.*(sin(t).*sin(p)).^2 +1).^1./6;
8 kspin = @(t,p) 5.*cos(t).^2.*sin(p).^2-2 ...
9 + (sin(t).^2.*sin(p).^2.*(10.*cos(t).^2.*sin(p).^2-1))./(3*sin(t).^2.*sin(p).^2+1);
10 g = @(t,p) kspin(t,p).*sin(p);
11
12 res = 100;
13 Q = zeros(res,1);
14 Q2 = zeros(res,1);
15
16 close all;
17 phi = (pi/2)*(1+(1:res)/res);
18 theta = ((1:res)-1)*2*pi/res;
19 phiedge=zeros(res);
20 phimax=zeros(res,1);
21 phimin=zeros(res,1);
22 Qmin=zeros(res,1);
23 Qmax=zeros(res,1);
24
25 for i=1:res
26     a = ((i+3)/(res+4)).^6;
27     phidet = @(t,phi) ( 3.*(sin(t).*sin(phi)).^2 +1).*(cos(phi).^6) - a );
28     edge = @(t) fzero2d(phidet,t);
29     phiedge(:,i) = edge(theta);
30     phimax = max(phiedge);%LELIJK!
31     phimin = min(phiedge);
32     Qmin(i) = integral2(g,0,2*pi,phimin(i),pi);
33     Qmax(i) = integral2(g,0,2*pi,phimax(i),pi);
34     Q(i) = integral2(g,0,2*pi,edge,pi);
35 end
36
37 hoogte =((4:(res+3))/(res+4));
38 figure();
39 hold on;
40 plot(hoogte , Q)
41 title('Total k_{spin} as function of magnetic field');
42 hold off;
```

```

43
44
45 res = 1000;
46 [X,Y,Z] = sphere(res-1);
47 [t,p,R] = cart2sph(X,Y,Z);
48 p = p((1:res/2),:);
49 t = t((1:res/2),:);
50 R = R((1:res/2),:);
51
52 R = r(t,pi/2-p);
53 Kspin = kspin(t,pi/2-p)./(r(t,pi/2-p).^2);
54
55 [X,Y,Z] = sph2cart(t,p,R);
56 close all;
57 set(0,'defaultTextFontName','Palatino');
58 set(0,'defaultAxesFontName','Palatino');
59 set(0,'defaultAxesFontSize',12);
60 set(0,'defaultTextFontSize',12);
61 fighandles(1)=figure();
62 mesh(X,Y,Z,Kspin,'Edgecolor','none','FaceColor','interp','FaceLighting','phong')
63 xlabel('x')
64 ylabel('y')
65 zlabel('z')
66 caxis([-3,3])
67 xlim([-1.5,1.5])
68 ylim([-1.5,1.5])
69 colormap(symmap);
70 hold off;
71
72 fighandles(2)=figure();
73 mesh(X,Y,Z,Kspin,'Edgecolor','none','FaceColor','interp','FaceLighting','phong')
74 xlabel('x')
75 ylabel('y')
76 zlabel('z')
77 xlim([-1.5,1.5])
78 ylim([-1.5,1.5])
79 colormap(symmap);
80 hold off;
81
82 Kspin = Kspin.*abs(cos(t).*cos(p));
83 fighandles(3)=figure();
84 mesh(X,Y,Z,Kspin,'Edgecolor','none','FaceColor','interp','FaceLighting','phong')
85 %camlight left
86 xlabel('x')
87 ylabel('y')
88 zlabel('z')
89 caxis([-3 3])
90 xlim([-1.5,1.5])
91 ylim([-1.5,1.5])
92 colormap(symmap);
93 hold off;
94 end
95
96 function philim = fzero2d(twoargfun,t)
97     [n,m] = size(t);
98     philim = zeros(n,m);
99     for i=1:n
100         for j=1:m
101             philim(i,j) = fzero(@(p) twoargfun(t(i,j),p) , 0.6.*pi);
102         end
103     end
104 end

```

mrfmsignal.m

This code calculates the integral as given by equations (2.8) and (2.9) for one specific set of values for the parameters. Wrapper codes such as wrapper.m can be used to produce relevant plots.

```

1 function [Kspin] = mrfmsignal(varargin)
2 %Calculates the expected Kspin signal assuming full saturation using a
3 %numerical computation of the dimensionless integral over the analytic
4 %expression g(theta,phi) It takes the following arguments (with it's default
5 %values): d = 3.5e-6, T = 0.1, B = 0.0522, dsample = 0.3e-6,
6 %dslice = 0.1e-6, rhospin = 8.5e26

```

```

7 %Code is written by Tobias de Jong Last edited: 12 June 2014
8
9
10 %Default parameters for sample
11 %height above sample (m), Temperature (K), Resonant field (T), Sample
12 %thickness (m), resonant slice thickness (m), rhospin (m^-3)
13 defaults = [3.5e-6, 0.1, 0.0522, 0.3e-6, 0.1e-6, 8.5e26];
14 defaults(1:nargin) = cell2mat(varargin);
15
16 %argh!
17 d = defaults(1);
18 T = defaults(2);
19 B = defaults(3);
20 dsample = defaults(4);
21 dslice = defaults(5);
22 rhospin = defaults(6);
23
24
25 %Geometrical functions
26 r = @(theta,phi) (3.*(sin(theta).*sin(phi)).^2 +1).^1./6);%relative radius of the slice
27 kspin = @(theta,phi) 5.*cos(theta).^2.*sin(phi).^2-2 ...
28 + (sin(theta).^2.*sin(phi).^2.*(10.*cos(theta).^2.*sin(phi).^2-1))./(3*sin(theta).^2.*sin(phi).^2+1);
29 g = @(theta,phi) kspin(theta,phi).*sin(phi);
30
31 %Physical constants (SI)
32 mu0 = 4*pi*10^-7;
33 mNdFeB = 2.3224*10^-11;
34 mFePt = 0.6e-11;
35 muN = 5.05078324*10^-27;
36 muB = 9.27400968*10^-24;
37 kb = 1.3806488*10^-23;
38
39 pol = @(T,B) tanh((2*muN.*B)./(2.*kb.*T));
40
41
42 Qupper=0;
43 Qlower=0;
44 %Calculating the integral for different values
45 temp = ((4*pi.*B.*d.^3)./(mu0.*mNdFeB)).^2;
46 if (temp>0 && temp<0.992)%because numerical calculations hate edgcases
47 phidet = @(theta,phi) ( 3.*(sin(theta).*sin(phi)).^2 +1).*(cos(phi).^6) - temp );
48 edge = @(theta) fzero2d(phidet,theta);
49 %Exploit the symmetry in horizontal directions to greatly improve
50 %performance:
51 Qupper = 4*integral2(g,0,0.5*pi,edge,pi);
52 end
53 temp = ((4*pi.*B.*(d+dsample).^3)./(mu0.*mNdFeB)).^2;
54 if (temp>0 && temp<0.992)
55 phidet = @(theta,phi) ( 3.*(sin(theta).*sin(phi)).^2 +1).*(cos(phi).^6) - temp );
56 edge = @(theta) fzero2d(phidet,theta);
57 %Exploiting again the symmetry in horizontal directions:
58 Qlower = 4*integral2(g,0,0.5*pi,edge,pi);
59 end
60
61 %Convert dimensionless integral to signal
62 Kspin = (3*muN.*pol(T,B).*rhospin.*dslice.*B)'.*(Qupper-Qlower);
63 end
64
65 function philim = fzero2d(twoargfun,t)
66 %Accepts a function handle in two arguments and a maximally 2 dim array t,
67 %and returns the value of the second argument of the function for which the
68 %function, with values t in the first argument, is zero.
69 [n,m] = size(t);
70 philim = zeros(n,m);
71 for i=1:n
72 for j=1:m
73 philim(i,j) = fzero(@(p) twoargfun(t(i,j),p) , 0.6.*pi);
74 end
75 end
76 end

```

wrapper.m

This is an example of a wrapper file invoking `mrfmsignal.m` to generate data for some plots. This specific code generated plots 2.4, 2.5.

```

1 %Plots the expected mrfm-signal as a function of magnetic field and
2 % height above the sample for different temperatures using mrfmsignal.m
3 res = 77;
4 T = [0.1 1 4];
5 Kspin = zeros(1,res);
6 d = 3.5e-6;
7 B = linspace(0.005,0.055,res);
8
9 %Generate the legendentries and set some plot layouts
10 legendentries = cell(3,1);
11 for i=1:3
12     legendentries{i} = strcat('T = ', num2str(T(i)), 'K');
13 end
14 set(0,'defaultTextFontName', 'Palatino')
15 set(0,'defaultAxesFontName', 'Palatino')
16 set(0,'defaultAxesFontSize', 12)
17 set(0,'defaultTextFontSize', 12)
18
19 %Calculate signal as a function of B
20 for j=1:res
21     for i=1:3
22         Kspin(i,j) = mrfmsignal(d, T(i), B(j));
23     end
24 end
25
26 %Plot that
27 figure();
28 hold on;
29 plot(B,Kspin,'x-')
30 xlabel('B-{'res} (T)')
31 ylabel('k-{'spin} (Nm^{-1})')
32 legend(legendentries,'Location','SouthWest')
33 hold off
34
35 %Calculate signal as a function of height above sample d
36 B = 0.02;
37 d = linspace(1.75e-6,5e-6,res);
38 for j=1:res
39     for i=1:3
40         Kspin(i,j) = mrfmsignal(d(j), T(i), B);
41     end
42 end
43
44 %plot
45 figure();
46 hold on;
47 plot(d,Kspin,'x-')
48 xlabel('d (m)')
49 ylabel('k-{'spin} (Nm^{-1})')
50 legend(legendentries,'Location','SouthWest')
51 hold off
52
53 %Calculate signal for B*d^3 = constant
54 B = 0.042.*(3.5e-6/d).^3;
55 Kspinequal = zeros(1,res);
56 for j=1:res
57     for i=1:3
58         Kspinequal(i,j) = mrfmsignal(d(j), T(i), B(j));
59     end
60 end
61
62 %plot
63 figure();
64 hold on;
65 plot(B,Kspinequal,'x-')
66 xlabel('B-{'res} (T)')
67 ylabel('k-{'spin} (Nm^{-1})')
68 legend(legendentries,'Location','SouthWest')
69 hold off

```

wrappermultilayer.m

This is an example of a wrapper file invoking mrfmsignal.m to generate data for plots. This specific code generated plot 2.10.

```

1 %Uses mrfmsignal.m to simulate the signal for different layers lying

```

```
2 %directly on top of each other at depths layerdepth beneath the surface,
3 %and generates a figure with a nice legend.
4 res = 91;
5 T = 0.1;
6 d = 3.5e-6;
7 layerdepth = [0 3 6 9].*0.1e-6;
8 numlayers = size(layerdepth,2)-1;
9 Kspin = zeros(res,numlayers);
10 B = linspace(0,0.055,res);
11 legendentries = cell(numlayers,1);
12 tic
13 %Calculations
14 for j=1:(numlayers)
15     parfor i = 1:res
16         Kspin(i,j) = mrfsignal(d+layerdepth(j), T, B(i), layerdepth(j+1)-layerdepth(j));
17     end
18     legendentries{j} = strcat('layer depth= ', num2str(layerdepth(j)*1e9), 'nm');
19 end
20 toc
21
22 %Convert from Kspin to frequencyshift
23 Df = Kspin.*0.5.*3000./10^-4;
24
25 %Plotting
26 figure();
27 hold on;
28 plot(B,Df)
29 legend(legendentries,'Location','SouthWest')
30 xlabel('B (T)')
31 ylabel('\Delta f (Hz)')
32 hold off
```


References

- [1] C. L. Degen, M. Poggio, H. J. Mamin, C. T. Rettner, and D. Rugar, *Nanoscale magnetic resonance imaging*, Proceedings of the National Academy of Sciences **106**, 1313 (2009).
- [2] J. Cardellino, N. Scozzaro, M. R. Herman, A. J. Berger, C. Zhang, K. C. Fong, C. Jayaprakash, D. V. Pelekhov, and P. C. Hammel, *Observation of Pure Spin Transport in a Diamond Spin Wire*, ArXiv e-prints (2013).
- [3] G. H. C. J. Wijts, *Magnetic resonance force microscopy at milliKelvin temperatures*, Casimir PhD series, 2013.
- [4] A. Vinante, G. Wijts, O. Usenko, L. Schinkelshoek, and T. H. Oosterkamp, *Magnetic resonance force microscopy of paramagnetic electron spins at millikelvin temperatures*, Nat Commun **2**, 572 (2011).
- [5] S. Lee, E. W. Moore, and J. A. Marohn, *Unified picture of cantilever frequency shift measurements of magnetic resonance*, Physical Review B **85**, 165447 (2012).
- [6] A. M. J. den Haan, G. H. C. J. Wijts, F. Galli, O. Usenko, G. J. C. van Baarle, D. J. van der Zalm, and T. H. Oosterkamp, *Atomic resolution scanning tunneling microscopy in a cryogen free dilution refrigerator at 15 mK*, Review of Scientific Instruments **85**, (2014).
- [7] A. Vinante, A. Kirste, A. den Haan, O. Usenko, G. Wijts, E. Jeffrey, P. Sonin, D. Bouwmeester, and T. H. Oosterkamp, *High sensitivity SQUID-detection and feedback-cooling of an ultrasoft microcantilever*, Applied Physics Letters **101**, (2012).
- [8] A. Abragam, *The principles of nuclear magnetism: the international series of monographs on physics*, Oxford University Press, Oxford, 1961.
- [9] A. Z. Genack and A. G. Redfield, *Theory of nuclear spin diffusion in a spatially varying magnetic field*, Phys. Rev. B **12**, 78 (1975).

- [10] A. Vinante, G. Wijts, O. Usenko, L. Schinkelshoek, and T. H. Oosterkamp, *Supplementary material of Magnetic resonance force microscopy of paramagnetic electron spins at millikelvin temperatures*, *Nat Commun* **2** (2011).